

Star Formation from Turbulent Fragmentation

Ralf S. Klessen

UCO/Lick Observatory, University of California, Santa Cruz, CA
95064, U.S.A.

Max-Planck-Institut für Astronomie, Königstuhl 17, 69117 Heidelberg,
Germany

Abstract. Star formation is intimately linked to the dynamical evolution of molecular clouds. Turbulent fragmentation determines where and when protostellar cores form, and how they contract and grow in mass via accretion from the surrounding cloud material. Using numerical models of self-gravitating supersonic turbulence, efficiency, spatial distribution and timescale of star formation in turbulent interstellar clouds are estimated. Turbulence that is not continuously replenished or that is driven on large scales leads to a rapid formation of stars in a clustered mode, whereas interstellar turbulence that carries most energy on small scales results in isolated star formation with low efficiency. The clump mass spectrum for models of pure hydrodynamic turbulence is steeper than the observed one, but gets close to it when gravity is included. The mass spectrum of dense cores is log-normal for decaying and large-wavelength turbulence, similar to the IMF, but is too flat in the case of small-scale turbulence. The three-dimensional models of molecular cloud fragmentation can be combined with dynamical pre-main sequence stellar evolution calculations to obtain a consistent description of all phases of the star formation process. First results are reported for a one solar mass protostar.

1. Introduction

Stars are born in interstellar clouds of molecular hydrogen, and form by gravitational collapse of shock-compressed density fluctuations generated from the supersonic turbulence ubiquitously observed in molecular clouds (e.g. Elmegreen 1993, Padoan 1995, Klessen, Heitsch, & Mac Low 2000). Once a gas clump becomes gravitationally unstable, collapse sets in and the central density increases until a protostellar object forms which continues to grow in mass via accretion from the infalling envelope. As stars typically form in small aggregates or larger clusters (Lada 1992, Adams & Myers 2001) the interaction of protostellar cores and their competition for mass growth from their surroundings are important processes shaping the distribution of the final star properties.

Altogether star formation can be seen as a two-phase process: First, *turbulent fragmentation* leads to transient clumpy molecular cloud structure, with some of the density fluctuation exceeding the critical mass and density for gravitational contraction. This sets the stage for the second phase of star formation,

the *collapse of individual protostellar clumps* building up central protostars. To fully understand the star formation process and all its phases in detail is one of the fundamental challenges in astronomy. Describing the first phase of star formation requires the three-dimensional dynamical modeling of molecular cloud formation, evolution and fragmentation. In this contribution, I report results from numerical simulations using SPH, a particle-based approach to solve the equations of hydrodynamics. The method and its application to (driven or decaying) interstellar turbulence is introduced in §2 and §3. I demonstrate how supersonic turbulence may influence the properties of forming (proto)stellar aggregates and clusters, and discuss the spatial distribution and timescale of star formation in §4 and the expected mass spectra for gas clumps and protostars in §5. Finally, in §6 a first attempt to combine *all* phases of star formation into a consistent numerical scheme is presented.

2. SPH – A Particle-Based Flexible Method to Hydrodynamics

To adequately describe turbulent fragmentation and the formation of protostellar cores, it is necessary to resolve the collapse of shock compressed regions over several orders of magnitude in density. Due to the stochastic nature of supersonic turbulence, it is not known in advance where and when local collapse occurs. Hence, SPH (*smoothed particle hydrodynamics*) is used to solve the equations of hydrodynamics. It is a Lagrangian method, where the fluid is represented by an ensemble of particles and thermodynamical observables are obtained by averaging over an appropriate subset of the SPH particles (Benz 1990). High density contrasts are resolved by simply increasing the particle concentration where needed. SPH can also be combined with the special-purpose hardware device GRAPE (Sugimoto et al. 1990, Ebisuzaki et al. 1993, Steinmetz 1996) allowing for calculations at supercomputer level on a normal workstation. The simulations presented here concentrate on subregions within a much larger cloud, therefore periodic boundary conditions are adopted (Klessen 1997). The high-density cores of collapsing gas clumps are substituted by ‘sink’ particles (Bate, Bonnell & Price 1995) while keeping track of mass and momentum. This allows for following the dynamical evolution of the system over many free-fall timescales.

3. Models of Driven Supersonic Turbulence

The large observed linewidths in molecular clouds imply the presence of supersonic velocity fields that carry enough energy to counterbalance gravity on global scales (Williams, Blitz, & McKee 2000). However, it is known that turbulent energy dissipates rapidly, roughly on the free-fall timescale (Mac Low et al. 1998, Stone, Ostriker, & Gammie 1998, Padoan & Nordlund 1999). Unlike previously thought, this is independent of the presence of magnetic fields. The fields are therefore taken as being dynamically unimportant in the current models, and are not included. To prevent or considerably postpone global collapse, turbulence must be continuously replenished. This is achieved by applying a Gaussian driving scheme, that inserts kinetic energy in a specified range of wavenumbers k . I select $1 \leq k \leq 2$, $3 \leq k \leq 4$, and $8 \leq k \leq 8$, corresponding to sources that

act on large, intermediate, and small scales, respectively. The energy input at each timestep is adjusted to reach a constant level of the total kinetic energy sufficient to stabilize the cloud as a whole (Mac Low 1999). Furthermore one molecular cloud model is considered where turbulence is assumed to have decayed, leaving behind Gaussian density fluctuations which begin to contract on all scales. For details see Klessen (2001).

The models presented here are computed in normalized units. If scaled to mean densities of $n(\text{H}_2) = 10^4 \text{ cm}^{-3}$, a value typical for star-forming molecular cloud regions (e.g. in ρ -Ophiuchus, see Motte, André, & Neri 1998) and a temperature of 11.4 K (i.e. a sound speed $c_s = 0.2 \text{ km/s}$), then the total mass contained in the computed volume is $413 M_\odot$ and the size of the cube is 0.89 pc. It contains 64 thermal Jeans masses.

4. Spatial Distribution and Timescale of Star Formation

Stars form from turbulent fragmentation of molecular cloud material. Supersonic turbulence that is strong enough to counterbalance gravity on global scales will usually provoke *local* collapse. Turbulence establishes a complex network of interacting shocks, where converging shockfronts generate clumps of high-density. This density enhancement can be large enough for the fluctuations to become gravitationally unstable and collapse, i.e. when the local Jeans length becomes smaller than the size of the fluctuation. However, the fluctuations in turbulent velocity fields are highly transient. The random flow that creates local density enhancements can disperse them again. For local collapse to actually result in the formation of stars, locally Jeans unstable, shock-generated, density fluctuations must collapse to sufficiently high densities on time scales shorter than the typical time interval between two successive shock passages. Only then are they able to ‘decouple’ from the ambient flow pattern and survive subsequent shock interactions. The shorter the time between shock passages, the less likely these fluctuations are to survive. Hence, the efficiency of protostellar core formation and the rate of continuing accretion onto collapsed cores depend strongly on the wavelength and strength of the driving source (see Klessen et al. 2000, Heitsch, Mac Low, & Klessen 2001).

The velocity field of long-wavelength turbulence is dominated by large-scale shocks which are very efficient in sweeping up molecular cloud material, thus creating massive coherent structures. When a coherent region reaches the critical density for gravitational collapse its mass typically exceeds the local Jeans limit by far. Inside the shock compressed region, the velocity dispersion is much smaller than in the ambient turbulent flow and the situation is similar to localized turbulent decay. Quickly a cluster of protostellar cores builds up. Both, decaying and large-scale turbulence lead to a *clustered* mode of star formation. The efficiency of turbulent fragmentation is reduced if the driving wavelength decreases. When energy is carried mainly on small spatial scales, the network of interacting shocks is very tightly knit, and protostellar cores form independently of each other at random locations throughout the cloud and at random times. Individual shock generated clumps have lower mass and the time interval between two shock passages through the same point in space is small. Hence, collapsing cores are easily destroyed again and star formation is inefficient. This

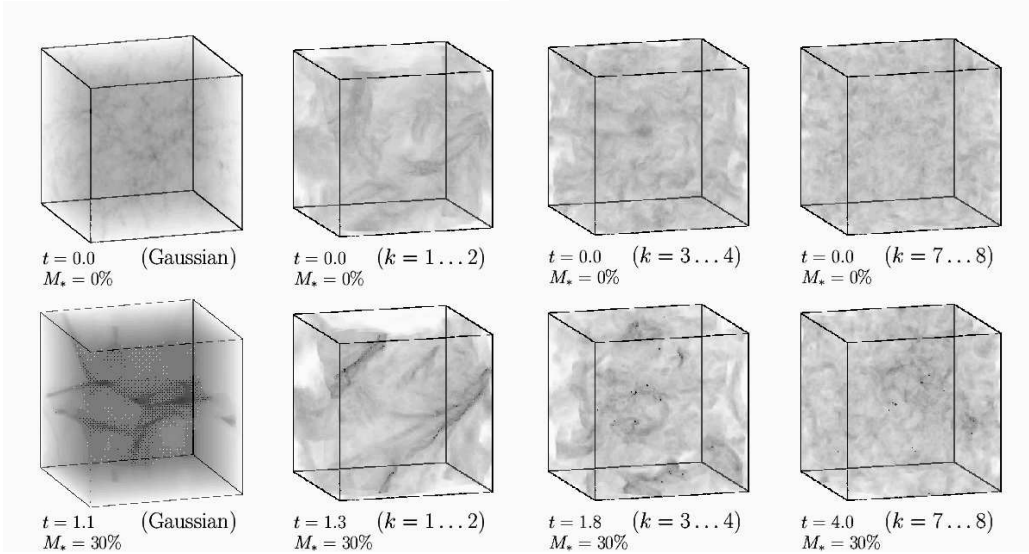


Figure 1. Comparison of the gas distribution in the four models: decayed turbulence leading to a Gaussian field (left column), large-scale turbulence (second column), intermediate-wavelength turbulence (third column), and small-wavelength turbulence (right column). The upper panel depicts the initial stage when gravity is ‘turned on’, the lower panel shows system after the first cores have formed and accumulated roughly 30% of the total mass.

scenario corresponds to the *isolated* mode of star formation. It needs to be pointed out that there is no fundamental dichotomy between the two modes of star formation, they rather define the extreme ends in the continuous spectrum of the properties of turbulent molecular cloud fragmentation.

This is visualized in Fig. 1. It compares the models of decayed, large-wavelength ($k = 1 \dots 2$), intermediate ($k = 3 \dots 4$), and small-scale turbulence ($k = 7 \dots 8$). The density structure of the systems is depicted at $t = 0$, which means for the model of decayed turbulence that the initial Gaussian density field is visible. For the driven models, $t = 0$ corresponds to the phase of fully developed turbulence just before gravity is ‘switched on’. The lower panel describes the four models after the first protostellar cores have formed via turbulent fragmentation and have accreted 30% of the total mass. Time is measured in units of the global free-fall timescale. Dark dots indicate the location of dense collapsed core. As for decayed turbulence all spatial modes are unstable, the system quickly evolves into a network of intersecting filaments, where protostellar cores predominantly form. Similarly, also large-scale turbulence builds up a network of filaments, however, this time the large coherent structures are not caused by gravity, but instead are due to shock compression. Once gravity is included, it quickly dominates the evolution inside the dense regions and again a cluster of protostellar cores builds up. In the case of intermediate-wavelength turbulence, cores form in small aggregates, whereas small-scale turbulence leads to local collapse of individual objects randomly dispersed throughout the volume. Note the different times needed for 30% of the mass to be accumulated in

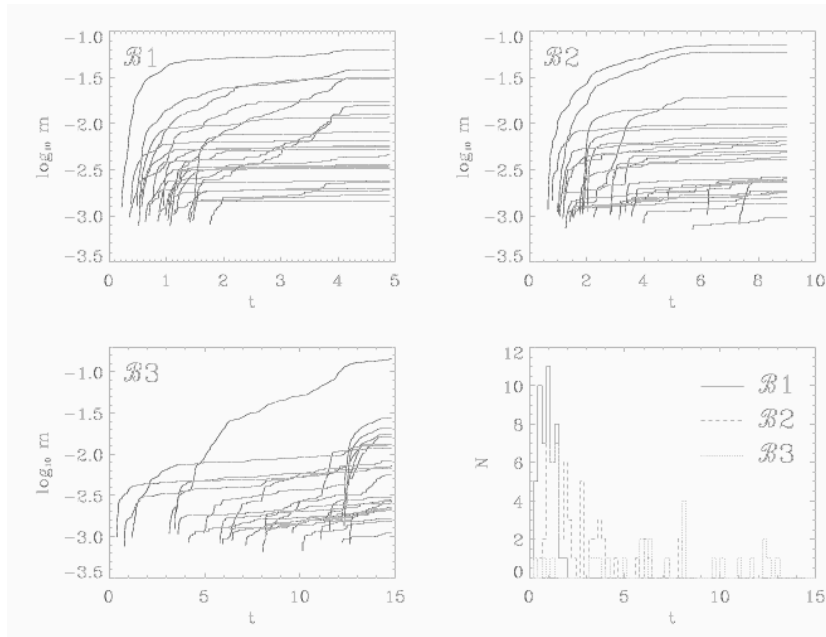


Figure 2. Mass growth history of protostellar cores (only every second core is depicted): long-wavelength ($\mathcal{B}1h$), intermediate- ($\mathcal{B}2h$), and small-scale turbulence ($\mathcal{B}3h$). The lower left plot shows the distribution of the formation times of the cores. Time is given in units of the free-fall time and masses are scaled to the total mass in the system.

dense cores. For small-scale turbulence star formation needs longest and speeds up with increasing wavelength, and as expected the rates for large-scale turbulence and locally decayed turbulence are comparable. This is also seen in Fig. 2, which shows the mass accretion history of individual protostellar cores for the three turbulent models, together with the distribution of core formation times. Star formation efficiency is high in the long-wavelength model, all cores form within two free-fall times, whereas in the short-wavelength model the efficiency is low and core formation continues for over 15 free-fall timescales (when the simulation was stopped).

5. Mass Spectra of Clumps and Protostellar Cores

The dominant parameter determining stellar evolution is the mass. It is therefore important to investigate the relation between the masses of molecular clumps, protostellar cores and the resulting stars. Figure 3 plots for the four models the mass distribution of all gas clumps, of the subset of Jeans critical clumps, and of collapsed cores. Four different evolutionary phases are shown, initially just when gravity is ‘switched on’, and after turbulent fragmentation has lead to the accumulation of $M_* \approx 5\%$, $M_* \approx 30\%$ and $M_* \approx 60\%$ of the total mass in dense cores.

In the initial, completely pre-stellar phase the clump mass spectrum is very steep (about Salpeter slope or less) at the high-mass end and gets shallower below $M \approx 0.4 \langle M_J \rangle$ with slope -1.5 , when using a power-law fit. The spectrum strongly declines beyond the SPH resolution limit. Altogether, individual clumps are hardly more massive than a few $\langle M_J \rangle$.

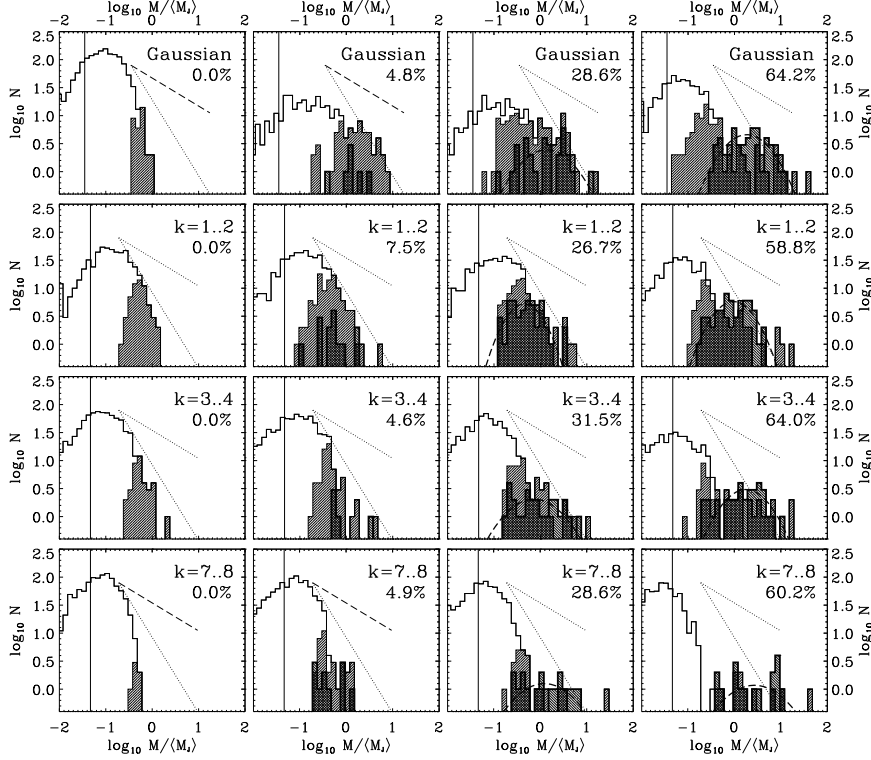


Figure 3. Mass spectra of dense collapsed cores (hatched thick-lined histograms), of gas clumps (thin lines), and of the subset of Jeans unstable clumps (thin lines, hatched distribution). Masses are binned logarithmically and normalized to the average Jeans mass $\langle M_J \rangle$. The left column gives the initial state of the system, just when gravity is ‘switched on’, the second column shows the mass spectra when roughly $M_* \approx 5\%$ of the mass is in dense cores, the third column when this fraction is about 30%, and the right column when $M_* \approx 60\%$. For comparison with power-law spectra ($dN/dM \propto M^\nu$), the typical slope $\nu = -1.5$ of the observed clump mass distribution, and the Salpeter slope $\nu = -2.33$ for the IMF, are indicated by the long dashed and by the dotted lines in each plot. The vertical line shows the SPH resolution limit.

Gravity strongly modifies the distribution of clump masses during the later evolution. As clumps merge and grow bigger, the mass spectrum becomes flatter and extends towards larger masses. Consequently the number of cores that exceed the Jeans limit grows, and local collapse sets in leading to the formation

of dense cores. This is most evident in the Gaussian model of decayed turbulence, where the velocity field is entirely determined by gravitational contraction on all scales. The clump mass spectrum in intermediate phases of the evolution (i.e. when protostellar cores are forming but the overall gravitational potential is still dominated by non-accreted gas) exhibits a slope -1.5 similar to the observed one. When the velocity field is dominated by strong (driven) turbulence, the effect of gravity on the clump mass spectrum is much weaker. It remains steep, close to or even below the Salpeter value. This is seen for small-wavelength turbulence. Here, the short interval between shock passages prohibits efficient merging and the build up of a large number of massive clumps. Only few clumps become Jeans unstable and collapse to form cores. These form independent of each other at random locations and times and typically do not interact. Increasing the driving wavelength leads to more coherent and rapid core formation, which also results in a larger number of cores. It is maximum in the case of pure gravitational contraction (decayed turbulence).

Long-wavelength turbulence or turbulent decay leads to a core mass spectrum that is well approximated by a *log-normal*. It roughly peaks at the *average thermal Jeans mass* $\langle M_J \rangle$ of the system and is comparable in width with the observed IMF (see Klessen & Burkert 2000, 2001). The log-normal shape of the mass distribution may be explained by invoking the central limit theorem (e.g. Zinnecker 1984), as protostellar cores form and evolve through a sequence of highly stochastic events (resulting from supersonic turbulence and/or competitive accretion). To find the mass peak at $\langle M_J \rangle$ may be somewhat surprising given the fact that the local Jeans mass strongly varies between different clumps. In a statistical sense the system retains knowledge of its mean properties. The total width of the core distribution is about two orders of magnitude in mass and is approximately the same for all four models. However, the spectrum for intermediate and short-wavelength turbulence, i.e. for isolated core formation, is too flat (or equivalently too wide) to be comparable to the observed IMF. This is in agreement with the hypothesis that most stars form in aggregates or clusters.

6. Towards an Integral Description of Star Formation

Three-dimensional calculations of molecular cloud dynamics can only describe the first phases of the star formation process: turbulent molecular cloud fragmentation and formation of collapsing protostellar cores. These calculation fail to resolve the build-up of the protostar itself. Understanding the temporal evolution of its structural parameters and the determination of observables like luminosity and effective temperature as the star approaches the main sequence requires detailed protostellar evolutionary calculations. These calculations are important, because they give ages, masses and radii of young stars when brightness, distance and effective temperature are known. The so determined ages constitute the only practical ‘clock’ for tracing the history of star-formation regions and for studying the evolution of circumstellar disks and planet formation.

However, almost all classical PMS calculations start *after* the main protostellar accretion phase ended. Formation and mass growth of the protostar are usually neglected, and its internal thermal structure is taken to be fully

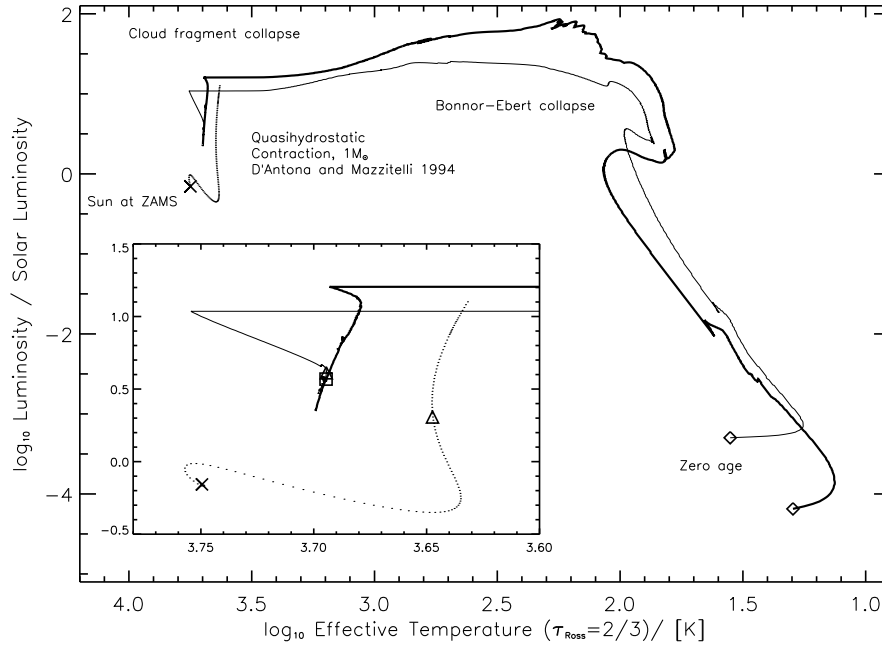


Figure 4. Early stellar evolution in the Hertzsprung-Russell diagram. Three evolutionary effective-temperature-luminosity relations (tracks) relevant to the young Sun are compared. The dotted line is a classical stellar structure, hydrostatic-equilibrium PMS-track for $1 M_{\odot}$, for an initially fully convective gas sphere (‘MLT Alexander’ model of D’Antona & Mazzitelli 1984). The two other lines are obtained by describing the formation of the star as a result of the collapse of an interstellar cloud. The *thin line* is for a cloud fragment in initial equilibrium (a so called ‘Bonnor-Ebert’ sphere of a solar mass, see Wuchterl & Tscharnuter 2001 for details). The (*thick line*) is for a cloud fragment that results from the dynamical fragmentation of a molecular cloud (model \mathcal{I} of Klessen & Burkert 2000, see Wuchterl & Klessen 2001 for details). The two diamonds, in the lower right, indicate zero age for the two collapse-results, when the protostellar fragments for the first time become optically thick and depart from isothermality. Triangles and squares mark the point along the respective evolutionary tracks where an age of 1 million years is reached. The cross on the hydrostatic track denotes the moment when energy generation by nuclear reactions in the stellar interior, for the first time in stellar live *fully* compensates the energy losses due to radiation from the stellar photosphere, i.e. the zero age main sequence (ZAMS). Note, that once accretion fades away the dynamical PMS calculations converge and predict that the proto-Sun was 500 K hotter and twice as luminous as in the classical hydrostatic model. The figure is a courtesy of G. Wuchterl.

convective (e.g. D'Antona & Mazzitelli 1994). However, it has been shown recently that protostellar collapse does *not* lead to a fully convective stellar structure when calculated consistently, taking into account radiation-hydrodynamics, time-dependent convection and nuclear burning processes (Wuchterl & Tscharnuter 2001).

A fully *consistent* treatment of formation and evolution of protostars requires coupling the 3D cloud fragmentation models with the 1D dynamical description of protostellar collapse. This can be achieved by taking the physical parameters and the time dependent mass accretion rates onto individual protostellar cores from the 3D model as boundary values for the detailed 1D calculation (see Wuchterl & Klessen 2001). For the proto-Sun, i.e. a cloud fragment with $1 M_{\odot}$, the evolutionary path in the Hertzsprung-Russell (HR) diagram is illustrated in Fig. 4.

These calculations demonstrate that luminosity and temperature of protostars not only depend on mass and age, but also on the accretion rate in the main accretion phase. Therefore, the position of a protostar on the HR diagram is sensitive to the cluster environment, because stochastic core interaction and competition strongly influence the mass accretion rate: *PMS tracks are not unique, and mass (or similarly age) of individual protostars from using the HR diagram can only be determined in a statistical sense.*

Furthermore, the new dynamical models predict considerable differences to the currently established classical PMS tracks: Instead of being fully convective, the structure of a $1 M_{\odot}$ protostar is homologous to the present day Sun. Already an age of 1 million years, it has a radiative core and a convective envelope. For this reason, the dynamical PMS calculations predict that the proto-Sun was 500 K hotter and twice as luminous as in the classical hydrostatic model. Altogether, conclusive observational tests are necessary to determine the validity of the numerical models. It is essential in this context to obtain independent mass and/or age determinations, e.g. from PMS binary stars or detailed modeling of protostellar disks (see Simon, Dutrey, & Guilloteau 2000, or Woitas, Köhler, & Leinert 2001 for first estimates).

Acknowledgments. I thank Günther Wuchterl, Mordecai-Mark Mac Low, Fabian Heitsch, and Peter Bodenheimer for many stimulating discussions and fruitful collaboration.

References

- Adams, F. C., Myers, P. C., 2001, ApJ, 553, 744
 Benz, W., 1990, in The Numerical Modeling of Nonlinear Stellar Pulsations, ed. J. R. Buchler (Dordrecht: Kluwer), 269
 Bate, M. R., Bonnell, I. A., Price, N. M., 1995, MNRAS, 277, 362
 D'Antona, F., Mazzitelli, I., 1994, ApJS, 90, 467
 Ebisuzaki, T., Makino, J., Fukushige, T., Taiji, M., Sugimoto, D., Ito, T., Okumura, S. K., 1993, PASJ, 45, 269
 Elmegreen, B. G., 1993, ApJ, 419, L29
 Heitsch, F., Mac Low, M.-M., Klessen, R. S., 2001, ApJ, 547, 280

- Klessen, R. S., 1997, MNRAS, 292, 11
Klessen, R. S., 2001, ApJ, 556, 837
Klessen, R. S., Burkert, A., 2000, ApJS, 128, 287
Klessen, R. S., Burkert, A., 2001, ApJ, 549, 386
Klessen, R. S., Heitsch, F., Mac Low, M.-M., 2000, ApJ, 535, 887
Lada, E., 1992, ApJ, 393, L25
Mac Low, M.-M., 1999, ApJ, 524, 169
Mac Low, M.-M., Klessen, R. S., Burkert, A., Smith, M. D., 1998, Phys.Rev.Lett, 80, 2754
Mizuno, A., Onishi, T., Yonekura, Y., Nagahama, T., Ogawa, H., Fukui, Y., 1995, ApJ, 445, L161
Motte, F., André, P., Neri, R., 1998, A&A, 336, 150
Padoan, P., 1995, MNRAS, 277, 337
Padoan, P., Nordlund, Å., 1999, ApJ, 526, 279
Steinmetz, M., 1996, MNRAS, 278, 1005
Simon, M., Dutrey, A., Guilloteau, S., 2000, ApJ, 545, 1034
Stone, J. M., Ostriker, E. C., Gammie, C. F., 1998, ApJ, 508, L99
Sugimoto, D., Chikada, Y., Makino, J., Ito, T., Ebisuzaki, T., Umemura, M., 1990, Nature, 345, 33
Williams, J. P., Blitz, L., McKee, C. F., 2000, in Protostars and Planets IV, eds. V. Mannings, A. Boss, & S. Russell (Tucson: Univ. of Arizona Press), 97
Woitias, J., Köhler, R., Leinert, C., 2001, A&A, 369, 249
Wuchterl, G., Tscharnuter, W. M., 2001, A&A, submitted
Wuchterl, G., Klessen, R. S., 2001, ApJ, 560, in press (astro-ph/0109051)
Zinnecker, H., 1984, MNRAS, 210, 43